NUMERICAL AERODYNAMIC-THERMAL-STRUCTURAL ANALYSES OF MISSILE FIN CONFIGURATION DURING SUPERSONIC FLIGHT CONDITIONS

Ognjen V. OGNJANOVIĆ [1], Stevan M. MAKSIMOVIĆ [1], Nenad D. VIDANOVIĆ [2,] *, Stevo D. ŠEGAN [3], Gordana M. KASTRATOVIĆ [2]

[1] Military Technical Institute, Ratka Resanovića 1, 11000 Belgrade, Serbia

[2] Faculty of Transport and Traffic Engineering, University of Belgrade, Vojvode Stepe 305, 11000 Belgrade, Serbia

[3] Faculty of Mathematics, University of Belgrade, Studentski Trg 16, 11000 Belgrade, Serbia

* Corresponding author; E-mail: n.vidanovic@sf.bg.ac.rs

Attention in this work is focused on aerodynamic heating and aero-thermo-mechanical analysis of fin type structures on the missile at supersonic flight. At high Mach number the heat due to friction between body and flow, i.e. viscous heating must be taken into account because the velocity field is coupled with the temperature field. The flow field around the fins of the missile and especially the temperature distribution on its surface, as well as aerodynamic-thermal-structural analyses are numerically modeled in ANSYS Workbench environment. The investigation was carried out for two Mach numbers (M = 2.3 and M = 3.7). Own available structural experimental results have been used for computational structural mechanics (CSM) validation and verification, in order to assure credibility of numerical fluid-thermal-structure interaction (FTSI). Conducted simulations were carried out to better understand the FTSIs of the missile fin during supersonic flight.

Key words: *Missile fins, Supersonic flight, Aerodynamic heating, Fluid-thermal-structure interaction*

1. Introduction

Aerodynamic heating is the heating of an aerospace vehicle which is occurring in very high speed exploitation regimes due to compression and friction within the boundary layer around the vehicle. Aerodynamic heating of supersonic and hypersonic flights has been under intensive consideration in recent years [1-12]. As a result of very high missile flight speeds, aerodynamic heating arises as a major problem to be considered in the missile design. This problem is larger near the stagnation regions, such as those existing at the missile fin leading edge [7-9, 12]. Also, one of the major issues, at supersonic flight conditions with higher Mach numbers, is that the fins can be subjected to substantial damage due to excessive heating and structural loading. So, investigation of aerodynamic heating coupled with aerodynamic force acting on the fin structure represents one of the major challenges in the design of supersonic and hypersonic vehicles, such as missile.

The approach to determine the missile aerodynamic characteristics may range from simple approximate, empirical, or semi-empirical analyses to detailed computational fluid dynamics (CFD) solutions. Studies that have improved numerical simulations enabled the solutions of complex multidisciplinary problems associated with projectile, missile and fin aerodynamics [10, 13-19].

Aerodynamic-thermal-structural analysis methods have an important role in the design of high speed flight vehicles and modelling of computational aerothermoelasticity phenomena, so they represent the necessary tool in aerospace design and optimization. Numerical prediction of thermally induced deformations and stresses [20] has been accomplished as a crucial sequence of spacecraft analysis [21].

It is obvious that the aero-heating problem requires aerothermoelastic analysis, which is based on multidisciplinary interaction between the elastic structure, heating and the aerodynamic and inertial forces acting on it, and its resulting behaviour and response during the exploitation. In order to provide the best possible design, opposite requirements imposed by aerothermoelasticity, i.e. aerodynamic, thermal and structural analyses have to be met.

In this multidisciplinary study numerical aerodynamic-structural and aerodynamic-thermal-structural analyses were carried out on a short range ballistic missile fin model, which was developed for scientific and internal experimental, CFD and CSM testing and calibration purposes. The design process of the ballistic missile fin model in question included primarily static structural experimental analyses, in order to achieve the maximal strength and safeness. Results of those experiments were used for validation and verification of CFD and CSM analyses of the missile fin model. Validation and verification procedures for numerical aerodynamic-structural analyses based on static structural experiments were a part of necessary routine, so that numerical aerodynamic-thermal-structural analyses could be carried out with acceptable accuracy.

The aim of this paper is to present a numerical aerodynamic-thermal-structural analyses of ballistic missile fin configuration during supersonic flight conditions, within a multipoint and multidisciplinary framework for aerodynamic-thermal-structural analyses, based on one multi-module software, in order to investigate thermal effects on fin structure, regarding safety and reliability in critical exploitation conditions and to improve and quicken the overall design processes with proposed numerical environment.

It should be noted that this study addresses a relevant aspect in missile aerothermoelasticity, because, as it can be seen from the presented literature survey, this kind of complex and robust analysis was never conducted on missile structures, since cited studies employ entirely different approaches. They use either custom made codes which generate aerodynamic databases based on curve fits of experimental data, 2D simplifications or semi-empirical methods, reduced order or theoretical methods or they are based on inviscid aerodynamic. Even if they uses commercial codes they use specialy developed data transfer interfaces.

2. Aerodynamic-thermal-structural environment

In this paper complete numerical analysis was performed in ANSYS Workbench environment. This multi-module software enables geometrical modelling, aerodynamic, thermal and structural analysis.

The algorithm of multimodular environment [15], for the purposes of computational aerodynamic-structural analysis and aerodynamic-thermal-structural analysis as well, is presented in Fig. 1. This algorithm shows data flows and order of activities in given automated framework.

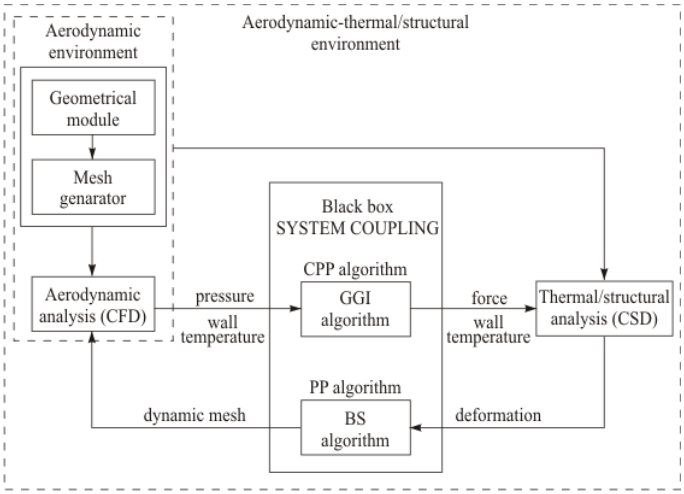

Figure 1. Multimodular environment dataflow algorithm

2.1. Geometrical module and mesh generator

The 3D parametric fin configuration and appropriate computational fluid domain were created in the DESIGN MODELER environment [22]. The fluid domain was modelled to be a part of paraboloid with 30 fin root chord lengths upstream and downstream from the tip of the model and with semi-axis of the paraboloid base with 30 fin root chord lengths, too. Boundary conditions for CFD analyses are defined as *wall*, *symmetry* and *pressure-far-field*. Boundary conditions for CSM analyses are defined as *Fluid Solid Interface* and *Fixed Support* or *Displacement*. These geometries delivered by DESIGN MODELER are discretized by MESH module [23]. These highly automated tools have been used for meshing structural and fluid domain.

2.2. Aerodynamic (CFD) and structural (CSM) analyses

For the air flow prediction the Navier-Stokes equations have to be solved. The three-dimensional, time-dependent, Reynolds Averaged Navier-Stokes equations are discretized using a cell-centreed finite volume approach. The entire system of governing equations in conservation form is as given in [24]. The flow solver, based on finite volume method, used in this study was the ANSYS FLUENT [25, 26]. Pressure-based type solver with coupled scheme was used to compute the flow field. The implicit formulation (coupled scheme) with Advection Upstream Splitting Method flux type was selected for solution method. The Least Square Cell Based for gradient, Second Order for pressure and the Second Order Upwind scheme for density, momentum, turbulent kinetic energy, specific dissipation rate and energy were selected for spatial discretization. Static temperature and static pressure were calculated with respect to their appropriate total values according to flow field Mach number. All surfaces of the models were defined as a stationary no-slip adiabatic wall conditions. Menter's [27-30] Shear Stress Transport k-ω model was selected for the numerical

calculation of the turbulent flow in the computational domain. The main control over the time-stepping scheme is the Courant number which was defined to be up to 200. Hybrid initialization method is used for each aerodynamic simulation initialization and represents the collection of instructions and boundary interpolation methods.

The structural solver, based on finite element method, used in this study was the ANSYS MECHANICAL (STATIC STRUCTURAL). Equilibrium equation for three dimensional static analysis problem was derived from the minimum potential energy principle [31]. The Sparse direct solver was used for the solutions of linear system of equations. This solver is primarily based on Gaussian elimination method used for obtaining unknown nodal displacements. For the lower-upper decomposition of quadratic global stiffness matrix Cholesky method was used, because sparse direct solver uses only non-zero matrix inputs.

2.3. System coupling

The SYSTEM COUPLING [32] module represents a special feature of multimodular environment which couples, controls and synchronizes selected solvers (modules) in order to complete all required coupled field analyses, which subsequently enables simulation of phenomena based on fluid-structure interaction. This feature enables transfer of properties and behaviours of analyzed fields in both directions, simulating two-way fluid-structure interaction (FSI) analysis, also two-way FTSI analysis, between two participants. To be more specific, closely coupling FSI and FTSI mechanism in this research was conducted [10, 33]. For the applied explicit model of analysis this iterative procedure is carried out only within the analyzed field loop of and the coupling field loop. This kind of analyses requires determination of the number of steps, which was defined to be 25, and number of iterations or convergence criteria in separate modules. For this kind of simulation model the equations which define fluid and structure are solved separately within the selected fluid and structural codes. Those equations are coupled in unique module which controls data transfer, creating realistic computational aerodynamic-structural and aerodynamic-thermal-structural procedure models, regarding the simulated phenomenon. After defining the type of simulation execution, it is necessary to couple solvers, define interacting regions and transfer variables. Next, it is necessary to select input/output variables (force, incremental displacement, temperature, heat flow rate, heat transfer coefficient, or near wall temperatures). This provides data transfer in both directions between solvers.

This kind of simulation required coupling of FLUENT and STATIC STRUCTURAL modules. The transfer variables which are being exchanged between defined regions and which correspond to the boundary conditions of *wall* (fluid domain) and *Fluid Solid Interface* (structure domain) are displacement increment, aerodynamic forces and temperature. Based on previously mentioned, it is necessary, within the FLUENT code, to provide remeshing of fluid domain in the moment of delivering calculated deformation from structural solver. In order to achieve mentioned condition, it was necessary for mesh moving/deforming of fluid domain technique to be employed within the two-way analysis. The dynamic mesh model, which is a part of FLUENT, has being used for simulations in cases when fluid domain mesh moving/deforming is caused by moving boundaries of other (structural) domain, which the fluid domain is in contact with.

Data transfer algorithms are combinations of mapping and interpolation algorithms that are used by the SYSTEM COUPLING module. Two mapping algorithms are in use for executing data

transfer procedures (Fig. 1). Data transfer procedure could be executed by *profile preserving* algorithm, when transferring non-conserved quantities (displacements or temperatures), and by *conservative profile preserving*, when transferring conserved quantities (mass, momentum, forces or energy flows). Within *profile preserving* algorithm the *Bucket Surface* mapping algorithm is used to generate mapping weights [34], while within *conservative profile preserving* algorithm the *General Grid Interface* mapping algorithm is used to generate mapping weights [35].

3. Numerical and experimental static structural analysis

Aerodynamic loads are defined for two cases (Tab. 1 and 2). The static structural analysis of the fin was experimentally tested for targeting flight condition (Tab. 2).

Table 1. Aerodynamic input data

Load case	H [m]	T [K]	M	AoA [^{o}]	a_x [ms^{-2}]	a_y [ms^{-2}]	g [ms^{-2}]
Case 1	10200	221.7	2.3	5	36.11	2.3	9.81
Case 2	18880	216.5	3.7	5	53.81	3.85	9.81

Table 2. Summary of CFD generated aerodynamic responses

Aerodynamic output data	Load case	
	Case 1	Case 2
Nominal aerodynamic force	F_L=3508.0 [N]	F_L=1418.0 [N]
Location of aerodynamic force (*X* axis)	0.4408 [m]	0.4516 [m]
Location of aerodynamic force (*Z* axis)	0.2276 [m]	0.2196 [m]

Based on the maximum aerodynamic lift force aspect one critical load case (Case 1, Tab. 2) is used in stress and strength analysis. Geometrical characteristics and material (Perunal 205-T6) properties for fin model are presented in Tab. 3 [36-38]:

Table 3. Geometrical characteristics and material properties for fin

Fin span:	0.500 [m]	Density:	2780 [kgm^{-3}]
Root chord length:	0.715 [m]	Poisson coefficient:	0.33
Tip chord length:	0.285 [m]	Young's modulus:	740 [GPa]
Angle between l. e. and *z*-axis:	40.69 [°]	Ultimate Tensile strength:	450 [MPa]
Root thickness:	0.0143 [m]	Yield strength:	300 [MPa]
Tip thickness:	0.0057 [m]	Coefficient of thermal expansion:	$2.4x10^{-5}$ [K^{-1}]
Fin area:	0.5024 [m^2]	Thermal conductivity:	156 [$Wm^{-1}K^{-1}$]
Mass:	6.79 [kg]	Specific heat:	963 [$Jkg^{-1}K^{-1}$]

2.3. Experimental installation for static tests of fin

Static structural experimental analysis of fin [36, 37] was carried out at Military Technical Institute in Belgrade. The experimental installation for static structural analysis of fin with analyzed model is shown in Fig. 2 (a). Same figure presents the manner in which the load is applied, and the transducers locations distribution (Fig. 2 (b)). Analyzed fin geometry is presented in Fig. 2 (c).

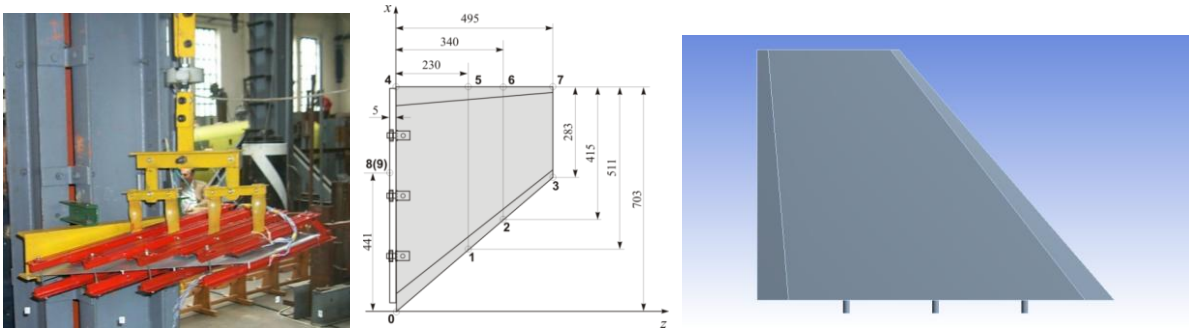

(a) **(b)** **(c)**

Figure 2. The experimental installation for static test of fin model (a), transducers displacements distribution presented in millimetres (b) and analyzed fin geometry (c)

For both Case 1 and Case 2 flight conditions, defined with the same critical angle of attack (AoA) value, the aerodynamic load of the fin (lift force) was obtained by panel method and verified by CFD code, and the agreement between those results was very good. After a well-conducted CFD validation/verification this result was accepted as credible. Calculated maximal load was applied on the model and the deformation was experimentally determined. The maximal displacement values were measured on locations 3 and 7 (Fig. 2 (b)), and they are u_3 = 0.01815 m and u_7 = 0.01925 m. These displacements correspond to the load case of maximal lift component F = 3508 N (Case 1) and were used for the purpose of CSM validation. The lift component value of F = 1418 N represents the second aerodynamic load case (Case 2).

In order to achieve as accurate results as possible, previous analysis included independently conducted static structural experiments of the analysed missile fin model. These experimental results, supported by panel and CFD analyses, were, in fact, the only available results, because the used experimental installation was not equipped with the devices for behaviour monitoring of aeroelastic structure, nor for aerothermal load analysis of any kind.

2.4. Verification, validation and numerical efficiency of CFD and CSM

The fin geometry was used for both CFD and CSM solver verification/validation. Verification of numerical aerodynamic results prediction, for five different mesh resolutions, was conducted for load case defined with Mach number 2.3 (Tab. 4). As it can be seen from Tab. 2, this load case delivered greater value of the lift force component, so based on the test demand this load case was used for static structural experiment. For all mesh resolutions the boundary layer was modeled with 20 layers and 1.2 growth rate and the height of the first cell was chosen to give y^+ value of about 1.0.

Table 4. Comparative review of aerodynamic responses with respect to five different discretizations of fluid domain

Number of cells	Calculated lift force [N]	Calculated location of aerodynamic force (*X*/*Z*) [m]	Duration of conducted simulation [min]
153195	3600.8	0.4289/0.2206	14
368634	3600.0	0.4268/0.2206	19
726948	3601.1	0.4247/0.2202	25
1413121	3605.4	0.4253/0.2203	40
3378599	3610.3	0.4258/0.2206	75

It is clearly to conclude that discrepancies between values of aerodynamic responses for Case 1 (Tab. 2) and obtained numerical values are small and acceptable. These numerical values are very similar among each other, so one can conclude that CFD results are more credible than panel method ones. Also, differences between CFD computing times are evident (Tab. 4). For the purpose of aerodynamic-structural simulation, number of cells of 368634 was chosen as optimal number of cells for fluid domain discretization, since in this case calculated lift force is the closest to the result obtained by CFD generated value used for structural experimental analysis (Tab. 2).

Results of conducted validation procedure of structural solver, based on experimentally obtained displacements on location 3 and location 7, are presented in Tab. 5. This table represents the differences between values of generated displacements at mentioned locations and the calculation times for four mesh resolutions of structural domain.

Table 5. Comparative review of calculated displacements with respect to four different discretizations of structural domain

Number of nodes	Calculated displacement on locations 3 and 7 (u_3/u_7) [mm]	Duration of conducted simulation [min]
61783	17.11/19.23	14
110267	17.15/19.27	19
393850	17.25/19.40	75
673471	17.29/19.43	160

The discrepancies between obtained structural responses are acceptable with respect to experimentally obtained ones, but calculating times are considerably different. Based on calculated displacement values (Tab. 5), for the purpose of aerodynamic-structural simulation, number of elements of 66194 (110267 nodes) was chosen as optimal number of elements for structural domain discretization. This locally conducted multidisciplinary study for fin geometry clearly suggests that in case when fluid domain was discretized with 368634 cells, and structural domain with 110267 nodes, time needed for static aeroelastic numerical calculations is optimal, with well-established numerical calculations accuracy. For the purpose of aerodynamic-structural simulations, structural domain was modelled with SOLID187 structural element. The difference regarding the lift calculated with panel method was 2.62 %, which leads to conclusion that numerical aerodynamic-structural model is very acceptable.

It should be noted that the differences between experimentally and numerically obtained displacements on positions 7 and 3 are 0.1 %, and 5.5 %, respectively. The difference on position 3 can be explained with coarse approximation of fin-body attachment.

3. Results and Discussion

In this section, results of numerical aerodynamic-structural, aerodynamic-thermal-structural and thermal-structural analyses are presented. Aerodynamic and structural responses, together with simulations execution times, are presented in tables, while the equivalent von-Mises stress distributions and temperature distributions are presented in figures.

3.1. Aerodynamic-structural analyses

In accordance with results of conducted numerical verification and validation procedures based on the fin static structural experiment for M = 2.3 and AoA = 5°, it can be concluded that with identical settings for numerical structural analyses of fin for M = 3.7 and AoA= 5°, for which static structural experiment was not conducted, can provide results that are reliable and accurate enough. Aerodynamic-structural numerical responses for both exploitation regimes (Case 1 and 2) are presented in Tab. 6.

Table 6. Aerodynamic-structural numerical responses for M = 2.3 and M = 3.7 exploitation regimes

M	AoA [°]	Calculated lift force [N]	Calculated location of aerodynamic force (X/Z) [m]	Calculated displacement on locations 3 and 7 (u_3/u_7) [mm]	Duration of conducted simulation [min]
2.3	5	3600.0	0.4268/0.2206	17.15/19.27	19
3.7	5	1522.3	0.4261/0.2171	7.02/7.96	19

For aerodynamic-structural analysis, equivalent von-Mises (averaged) stress distributions for both exploitation regimes are shown in Fig. 3. As it can be seen (Fig. 3 (a) and (c)), region of maximal stress was occurred on the third support. Numerical calculations of aerodynamic-structural behaviour consumed up to 6.63 GB RAM.

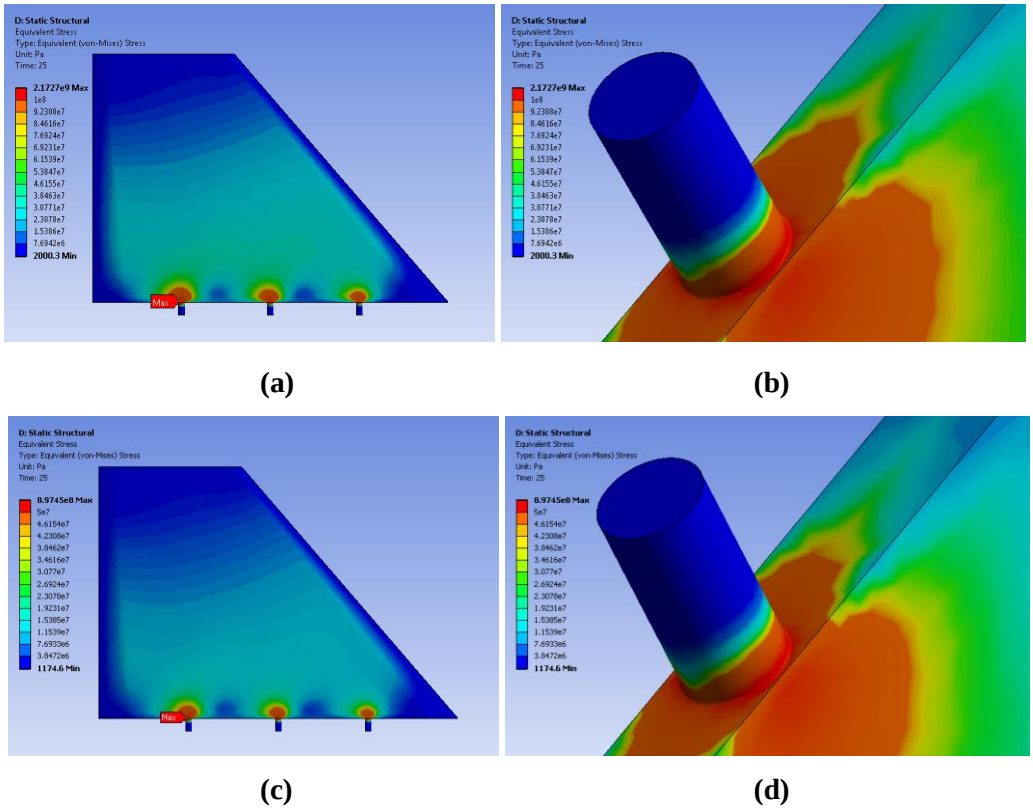

Figure 3. Stress distribution without thermal influence for M = 2.3 ((a) and (b)) and for M = 3.7 ((c) and (d))

3.2. Aerodynamic-thermal-structural analyses

Based on conducted studies, the optimal settings of numerical calculations have been adopted. The strategy is based on the assumption that if the validation/verification of aerodynamic-structural model (static aeroelastic) was very good, the aerodynamic-thermal-structural results of the analysed fin model are credible as well. So, the settings for aerodynamic-thermal-structural model are the same as the ones of static aeroelastic numerical model and with the same dicretizations of fluid and structural domain. For the purpose of aerodynamic-thermal-structural simulations, structural domain was modelled with SOLID227 coupled field element [39], which takes significantly longer to solve. The results of aerodynamic-thermal-structural analysis of fin for Case 1 and 2 are shown in Tab. 7.

Table 7. Aerodynamic-thermal-structural numerical responses for *M* = 2.3 and *M* = 3.7 exploitation regimes

M	AoA [°]	Calculated lift force [N]	Calculated location of aerodynamic force (*X*/*Z*) [m]	Calculated displacement on locations 3 and 7 (u_3/u_7) [mm]	Duration of conducted simulation [min]
2.3	5	3581.4	0.4151/0.2199	20.78/24.09	31
3.7	5	1501.5	0.4125/0.2125	14.17/17.46	26

For aerodynamic-thermal-structural analysis, equivalent von-Mises (averaged) stress distributions for both exploitation regimes are shown in Fig. 4. As it can be seen (Fig. 4 (a) and (c)), region of maximal stress was occurred on the first support. Numerical calculations of aerodynamic-thermal-structural behaviour consumed up to 8.43 GB RAM.

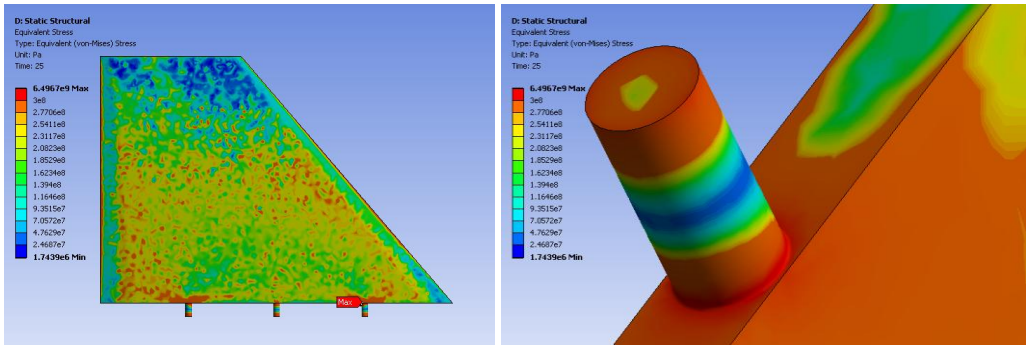

(a) **(b)**

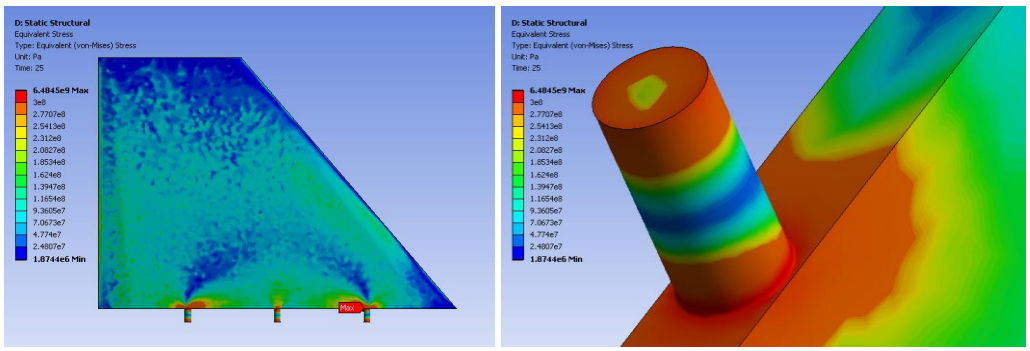

(c) **(d)**

Figure 4. Stress distribution with thermal influence for *M* = 2.3 ((a) and (b)) and for *M* = 3.7 ((c) and (d))

3.3. Thermal-structural analyses

Thermal-structural analysis takes into consideration only thermal influences. To be more specific, aerodynamic forces were excluded from transfer data within system coupling module, which means that the lift force was calculated in aerodynamic module but not delivered to structural module. Only calculated temperatures were exported. The aim of thermal-structural analysis was to point out the influence of temperature on structural behavior of analyzed exploitation regimes. The results of thermal-structural analysis of fin for Case 1 and 2 are shown in Tab. 8.

Table 8. Thermal-structural numerical responses for *M* = 2.3 and *M* = 3.7 exploitation regimes

M	AoA [°]	Calculated lift force [N]	Calculated location of aerodynamic force (*X*/*Z*) [m]	Calculated displacement on locations 3 and 7 (u_3/u_7) [mm]	Duration of conducted simulation [min]
2.3	5	3758.1	0.4179/0.2223	4.59/6.35	19
3.7	5	1531.7	0.4129/0.2161	7.63/10.25	19

For thermal-structural analysis, equivalent von-Mises (averaged) stress distributions for both exploitation regimes are shown in Fig. 5 (a) and (b). Surrounding temperature fields for both regimes are presented in Fig. 5 (c) and (d). Numerical calculations of thermal-structural behaviour consumed up to 8.25 GB RAM.

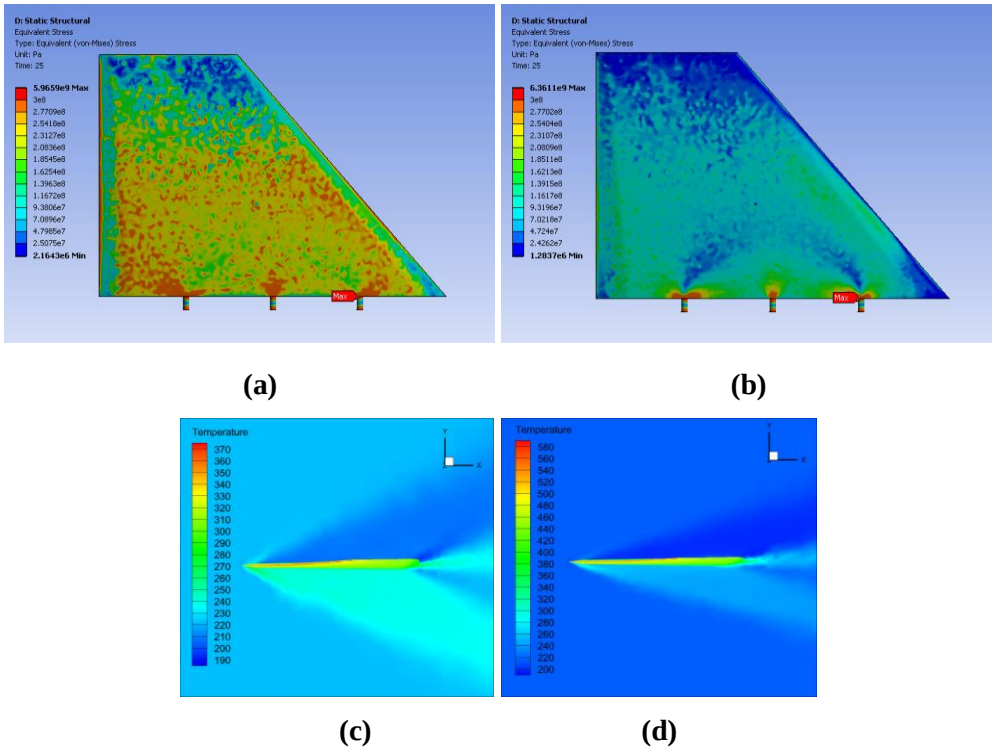

(a) **(b)**

(c) **(d)**

Figure 5. Stress distribution with solely thermal influence for *M* = 2.3 (a) and for *M* = 3.7 (b), and surrounding temperature fields for *M* = 2.3 (c) and *M* = 3.7 (d)

The static temperature distribution for M = 2.3 on fin surface is represent in Fig. 6 (a) and (b). The temperature change on whole fin surface is almost 124 K. As expected, temperatures are higher at the lower fin surface where is recorded the highest temperature of 380.412 K, which occurs directly beside the leading edge (Fig. 6 (a)). The temperatures are slightly lower at the upper fin surface (Fig. 6 (b)). Obviously, this temperature difference emanates from AoA, which is 5°, because the flow travels faster over the upper fin surface and the less heat is generated.

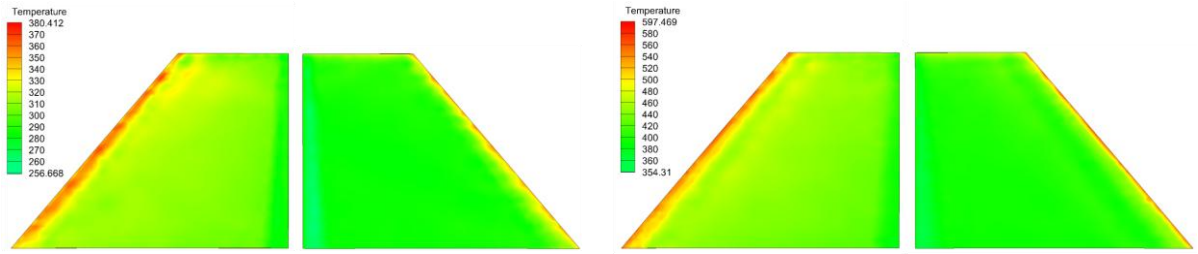

(a) **(b)** **(c)** **(d)**

Figure 6. Static temperature distribution for M = 2.3 on lower (a) and upper (b) fin surface and static temperature distribution for M = 3.7 on lower (c) and upper (d) fin surface

The static temperature distribution is also presented for M = 3.7 in Fig. 6 (c) and (d). In this case, the temperature change on whole fin surface is slightly above 243 K. Again, temperatures are higher at the lower fin surface, where is recorded the highest temperature of 597.469 K which occurs at the leading edge (Fig. 6 (c)), while the temperatures are slightly lower at the upper fin surface (Fig. 6 (d)), for the same reason as in previous case.

The displacements caused by aerodynamic heating are, obviously, greater than ones when aerodynamic heating is not taken into consideration. The maximum displacements in both cases occur at the same positions as the displacements without aerodynamic heating (Tab. 6 and 7). In case of M = 2.3 displacements are 21 % and 25 % greater for the location 3 and 7, respectively. But, those differences are much higher in case of M = 3.7: displacements are 201 % and 219 % greater for the location 3 and 7, respectively. Also, it is evident that increase in Mach number largely affects the increase in displacements.

It has to be noted, that due to coarse approximation of fin-body attachment, obtained equivalent stress values must be taken with great reserve. Never the less, these results can give the general picture of stress distributions in conducted analyses.

Similarly as displacements, the equivalent stresses are greater in case with aerodynamic heating taken into consideration, with the equivalent stress distributions nearly the same for both Mach numbers, but as it is shown in section 4.3 (Tab. 8 and Fig. 5 (a) and (b)) the influence of thermal stresses is greater for M = 3.7 than for M = 2.3. The maximum equivalent stresses appear on the first support from leading edge. In case without influence of aerodynamic heating, the equivalent stress distributions are different, whereby, as expected due to exploitation regimes, the maximum and minimum equivalent stresses are higher for M = 2.3 than for M = 3.7, with equivalent maximum stresses appear on the third support from leading edge.

It should be noted that in case when aerodynamic heating is taken into consideration, there is an increase in maximum stresses: 3 times for M = 2.3, and around 7 times for M = 3.7, while increase in

minimum stresses is significantly higher: several hundred times for M = 2.3 and over one thousand times for M = 3.7.

4. Conclusion

In this paper a multidisciplinary framework for numerical aerodynamic-thermal-structural analyses, based on only one multi-module software, was used to analyse thermal effects on fin structure during supersonic flights conditions. The analysis was conducted for two Mach numbers (M = 2.3 and M = 3.7). The obtained results showed evident influence of the Mach number on aerodynamic heating and stresses/displacements. The displacements and stresses in presence of aerodynamic heat were increased, but what was particularly interesting was the substantial increase in minimum stresses. Furthermore, the conducted analyses delivered qualitative results which can be used for fin material selection and improvement of fin support assembly.

The conduction of static structural experiments was a necessary condition to begin with creating well established numerical environment for aerodynamic-thermal-structural simulation, because they were used for validation and verification of CFD and CSM analyses of the missile fin model. Validation and verification enabled that the use of this numerical environment makes a significant upgrade of the overall fluid-thermal-structure interaction modelling and in quickening of the overall conceptual design process. The proposed well-established environment integrated with existing experimentally generated database represents powerful tool for numerical aerotermoelastic prediction in aerospace science and demonstrates high quality of modelled responses with acceptable calculation times.

So, this work describes the approach which can be adopted to estimate the aerodynamic heating effects on any aerodynamic configuration in spacecraft design, and hence to provide better general understanding of aerothermoelastic behaviour during supersonic flight conditions.

5. Nomenclature

$a_{x,y}$ - acceleration components, [ms^{-2}]
E - total energy, [J]
g - gravitational acceleration, [ms^{-2}]
H - altitude, [m]
k - turbulence kinetic energy, [m^{2}s^{-2}]
M - Mach number (=U/c), [-]
p - pressure, [Pa]
q_i - heat flux vector components, [Wm^{-2}]
T - temperature, [K]
u - x velocity component, [ms^{-1}]
$u_{3,7}$ - displacement on locations 3 and 7, [mm]
v - y velocity component, [ms^{-1}]
w - z velocity component, [ms^{-1}]
y^+ - dimensionless length parameter, [-]

Greek letters

α - coefficient of thermal expansion, [K^{-1}]
$\varepsilon_{i,j}$ - dilatation tensor components, [-]
ρ - density, [kgm^{-3}]
$\tau_{i,j}$ - viscous stress tensor components, [Pa]
ω - specific dissipation rate, [s^{-1}]

Acronyms

AoA - Angle of Attack, **[°]**
CFD - Computational Fluid Mechanics
CSM - Computational Structural Mechanics
FSI - Fluid Structure Interaction
FTSI - Fluid Thermal Structure Interaction

6. References

[1] Van Driest, E. R., The Problem of Aerodynamic Heating, *Aeronautical Engineering Review*, *15* (1956), 10, pp. 26-41

[2] Hopkins, E. J., Inouye, M., An Evaluation of Theories for Predicting Turbulent Skin Friction and Hypersonic Mach Numbers, *AIAA Journal*, *9* (1971), 6, pp. 993-1003

[3] Poll, D. I. A., An Introduction to the Problem of Aerodynamic Heating, Aeronautical Engineering Internal Report 8901, 1989

[4] Quinn, R. D., Gong, L., Real-Time Aerodynamic Heating and Surface Temperature Calculations for Hypersonic Flight Simulation, NASA Technical Memorandum, NASA-TM-4222, 1990

[5] Wurster, K. E., Stone, H. W., Aerodynamic Heating Environment Definition/Thermal Protection System Selection for the HL-20, *Journal of Spacecraft Rockets*, *30* (1993), 5, pp. 549-557

[6] Nishikawa, H., Aerodynamic Heating with Turbulent Flows, AE525 Research Project, 1994

[7] Mazzoni, J. A., Filho, J. B. P., Machado, H. A., Aerodynamic heating on VSB-30 sounding rocket, *Proceedings*, 18th International Congress of Mechanical Engineering, Ouro Preto, MG, November, 2005

[8] Mahulikar, S. P., Theoretical aerothermal concepts for configuration design of hypersonic vehicles, *Aerospace Science and Technology*, *9* (2005), pp. 681-685

[9] Cayzac, R., *et al.*, Navier-Stokes computation of heat transfer and aero-heating modeling for supersonic projectiles, *Aerospace Science and Technology*, *10* (2006), pp. 374-384

[10] Culler, A. J., Crowell, A. R., McNamara, J. J., Studies on Fluid-Structural Coupling for Aerothermoelasticity in Hypersonic Flow, *Proceedings*, 50th AIAA/ASME/ASCE/AHS/ASC Structures, Structural Dynamics, and Materials Conference, Palm Springs, California, May, 2009, AIAA Paper 2009-2364

[11] Kostoff, R. N., Cummings, R. M., Highly cited literature of high-speed compressible flow research, *Aerospace Science and Technology*, *26* (2013), pp. 216-234

[12] Bao, W., *et al.*, Effect of structural factors on maximum aerodynamic heat flux of strut leading surface, *Applied Thermal Engineering*, 69 (2014), pp. 188-198

[13] Ocokoljić, G. J., *at al.*, Aerodynamic shape optimization of guided missile based on wind tunnel testing and CFD simulation, *Thermal Science - Online First*, doi: 10.2298/TSCI1505151840

[14] Başkut, E., Akgül, A., Development of a Coupling Procedure for Static Aeroelastic Analyses, *Scientific Technical Review*, *61* (2011), 3-4, pp. 39-48

[15] Vidanović, N. D., Aerodynamic-structural optimization of aircraft lifting surfaces, Ph.D. thesis, (in Serbian), Faculty of Mechanical Engineering, University of Belgrade, Serbia, 2015

[16] Kroyer, R., FSI analysis in supersonic fluid flow, *Computers & Structures*, *81* (2003), pp. 755-764

[17] Friedmann, P. P., *et al.*, Aeroelastic analysis of hypersonic vehicles, *Journal of Fluids and Structures*, *19* (2004), pp. 681-712

[18] Seo, Y-J, *et al.*, Effects of multiple structural nonlinearities on limit cycle oscillation of missile control fin, *Journal of Fluids and Structures*, *27* (2011), pp. 623-635

[19] Firouz-Abadi, R. D., *et al.*, Analysis of non-linear aeroelastic response of a supersonic thick fin with plunging, pinching and flapping free-plays, *Journal of Fluids and Structures*, *40* (2013), pp. 163-184
[20] Ognjanović, O., Maksimović, K., Stamenković, D., Vasić, Z., The Effects of Thermal Gradients on Stress Distributions, *Proceedings*, 4th International Congress of Serbian Society of Mechanics, Vrnjačka Banja, Serbia, June, 2013, pp. 365-370
[21] Rašuo, B., *Aeronautical Safeguarding (VTOb)*, VIZ, Military Academy, Belgrade, 2004, (in Serbian)
[22] Design Modeler User's Guide, Release 15.0, ANSYS, Inc., November 2013.
[23] ANSYS Meshing User's Guide, Release 15.0, ANSYS, Inc., November 2013.
[24] Anderson, J. D., Jr., *Computational Fluid Dynamics, The Basics with Applications*, McGraw-Hill, Inc., Singapore, 1995
[25] ANSYS Fluent Theory Guide, Release 15.0, ANSYS, Inc., November 2013.
[26] ANSYS Fluent User's Guide, Release 15.0, ANSYS, Inc., November 2013.
[27] Menter, F. R., Two-Equation Eddy-Viscosity Turbulence Models for Engineering Applications, *AIAA Journal*, *32* (1994), 8, pp. 1598-1605
[28] Menter, F. R., Kuntz, M., Langtry, R., Ten Years of Industrial Experience with the SST Turbulence Model, in: *Turbulence, Heat and Mass Transfer 4* (Ed. K. Hanjalić, Y. Nagano, M. Tummers), Begell House, Inc., 2003, pp. 625-632
[29] Menter, F. R., Review of the shear-stress transport turbulence model experience from an industrial perspective, *International Journal of Computational Fluid Dynamics*, *23* (2009), 4, pp. 305-316
[30] Vidanović, N. D., *et al.*, Validation of the CFD code used for determination of aerodynamic characteristics of nonstandard AGARD-B calibration model, *Thermal Science*, *18* (2014), 4, pp. 1223-1233
[31] Rao, S. S., *The Finite Element in Engineering*, Elsevier, 2004
[32] System Coupling User's Guide, Release 15.0, ANSYS, Inc., November 2013.
[33] Kamakoti, R., Shyy, W., Fluid-structure interaction for aeroelastic applications, *Progress in Aerospace Sciences*, *40* (2004), pp. 535-558
[34] Jansen, K., Shakib, F., Hughes, T., Fast Projection Algorithm for Unstructured Meshes, in: *Computational Nonlinear Mechanics in Aerospace Engineering* (Ed. S. N. Atluri), American Institute of Aeronautics and Astronautics, 1992, pp. 175-204
[35] Galpin, P. F., Broberg, R. B., Hutchinson, B. R., Three-Dimensional Navier Stokes Predictions of Steady-State Rotor/Stator Interaction with Pitch Change, *Proceedings*, 3rd Annual Conference of the CFD Society of Canada, Banff, Alberta, Canada, June, 1995
[36] Maksimovic, S., *et al.*, Determination of Load Distributions on Main Helicopter Rotor Blades and Strength Analysis of the Structural Components, *Journal of Aerospace Engineering*, *27* (2014), 6
[37] Maksimovic, S., Stress and strength analysis of fin-test Model 1, No: 023-01-M, Internal report of Military Technical Institute, Belgrade, 2001
[38] Rašuo, B., *Aircraft Production Technology*, University of Belgrade, Faculty of mechanical engineering, Belgrade, 1995, (in Serbian)
[39] ANSYS Mechanical APDL Element Reference, Release 15.0, ANSYS, Inc., November 2013

Paper submitted: Sepetember 19, 2016
Paper revised: November 11, 2016
Paper accepted: November 29, 2016